

Generalized Parametric Contrastive Learning

Jiequan Cui, *Student Member, IEEE*, Zhisheng Zhong, *Student Member, IEEE*, Zhuotao Tian, *Student Member, IEEE*, Shu Liu, *Member, IEEE*, Bei Yu, *Member, IEEE*, Jiaya Jia, *Fellow, IEEE*

Abstract—In this paper, we propose the Generalized Parametric Contrastive Learning (GPaCo/PaCo) which works well on both imbalanced and balanced data. Based on theoretical analysis, we observe supervised contrastive loss tends to bias on high-frequency classes and thus increases the difficulty of imbalanced learning. We introduce a set of parametric class-wise learnable centers to rebalance from an optimization perspective. Further, we analyze our GPaCo/PaCo loss under a balanced setting. Our analysis demonstrates that GPaCo/PaCo can adaptively enhance the intensity of pushing samples of the same class close as more samples are pulled together with their corresponding centers and benefit hard example learning. Experiments on long-tailed benchmarks manifest the new state-of-the-art for long-tailed recognition. On full ImageNet, models from CNNs to vision transformers trained with GPaCo loss show better generalization performance and stronger robustness compared with MAE models. Moreover, GPaCo can be applied to semantic segmentation task and obvious improvements are observed on 4 most popular benchmarks. Our code is available at <https://github.com/dvlab-research/Parametric-Contrastive-Learning>.

Index Terms—Representation Learning, Contrastive Learning, OOD Robustness, Long-tailed Recognition, Semantic Segmentation.

1 INTRODUCTION

CONVOLUTIONAL neural networks (CNNs) have achieved great success in various tasks, including image classification [1], [2], object detection [3], [4] and semantic segmentation [5]. Especially, with the rise of neural network search [6], [7], [8], [9], [10], performance of CNNs have further taken a big step. However, The huge progress highly depends on large-scale and high-quality datasets, such as ImageNet [11], MS COCO [12] and Places [13]. But when deal with real-world applications, generally we face the long-tailed distribution problem – a few classes contain many instances, while most classes contain only a few instances. Learning in such an imbalanced setting is challenging as the low-frequency classes can be easily overwhelmed by high-frequency ones. Without considering this situation, CNNs will suffer from significant performance degradation.

Contrastive learning [15], [16], [17], [18], [19] is a major research topic due to its success in self-supervised representation learning. Khosla [20] extend non-parametric contrastive loss into non-parametric supervised contrastive loss by leveraging label information, which trains representation in the first stage and learns the linear classifier with the fixed backbone in the second stage. Though supervised contrastive learning works well in a balanced setting, for imbalanced datasets, our theoretical analysis shows that high-frequency classes will have a higher lower bound of loss and contribute much higher importance than low-frequency classes when equipping it in training. This phenomenon leads to model bias on high-frequency classes and increases the difficulty of imbalanced learning. As shown in Fig. 2,

when the model is trained with supervised contrastive loss on ImageNet-LT, the gradient norm varying from the most frequent class to the least one is rather steep. In particular, the gradient norm dramatically decreases for the top 200 most frequent classes.

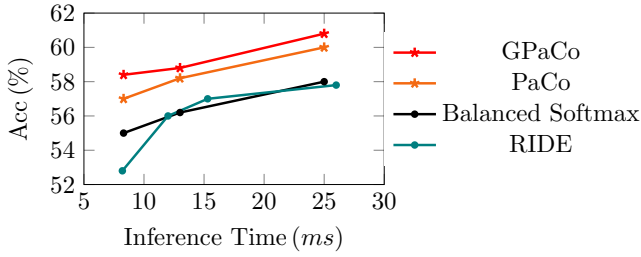
Previous work [21], [22], [23], [24], [25], [26], [27], [28], [29], [30], [30], [31], [32], [33] explored to rebalance in traditional supervised cross-entropy learning. In this paper, we tackle the above mentioned imbalance issue in supervised contrastive learning and make use of contrastive learning for long-tailed recognition.

To rebalance in supervised contrastive learning, we introduce a set of parametric class-wise learnable centers into supervised contrastive learning. We name our algorithm **Parametric Contrastive Learning (PaCo)** shown in Fig. 3 (a). With such a simple and yet effective operation, we theoretically prove that the optimal values for the probability that two samples are a true positive pair (belonging to the same class), varying from the most frequent class to the least frequent class, are more balanced. Thus their lower bound of loss values are better organized. This phenomenon means the model takes more care of low-frequency classes, making the PaCo loss benefit imbalanced learning. Fig. 2 shows that, with our PaCo loss in training, gradient norm varying from the most frequent class to the least one are moderated better than supervised contrastive learning, which matches our analysis.

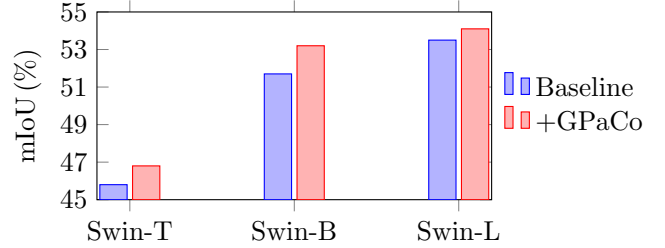
Further, we analyze the PaCo loss under a balanced setting. Our analysis demonstrates that with more samples clustered around their corresponding centers in training, the PaCo loss increases the intensity of pushing samples of the same class close, which benefits hard examples learning.

MoCo [16] enables small mini-batch training for self-supervised contrastive learning with a momentum encoder and a queue. [34] claims that it is the “stop-gradient” but not the momentum encoder that is necessary to avoid collapsing solutions for self-supervised learning. We examine the

- J. Cui, Z. Zhong, Z. Tian, B. Yu and J. Jia are with the Department of Computer Science & Engineering, The Chinese University of Hong Kong, ShaTin, Hong Kong.
E-mail: {jiekuan, tianzhuotao, liushuhust}@gmail.com
{zszhong21, byu, leojia}@cse.cuhk.edu.hk;
- J. Jia and S. Liu are with the SmartMore.



(a) Comparison on ImageNet-LT for long-tailed image classification.



(b) Comparison on ADE20K for semantic segmentation.

Models	ImageNet(\uparrow)	ImageNet-C(mCE \downarrow)	ImageNet-C(rel. mCE \downarrow)	ImageNet-R(\uparrow)	ImageNet-S(\uparrow)
ViT-B	+0.4	-1.9	-2.6	+1.8	+3.3
ViT-L	+0.3	-1.7	-2.4	+0.0	+2.8

(c) Comparison with MAE [14] ViT models on full ImageNet and out-of-distribution robustness.

Fig. 1. **GPaco demonstrates impressive performance on imbalanced and balanced data.** (a) shows that GPaco achieves state-of-the-art on long-tailed classification. GPaco benefits semantic segmentation task and significant improvement is observed on ADE20K in (b). In (c), top-1 accuracy are reported for full ImageNet, ImageNet-R, and ImageNet-S. mCE and rel. mCE are used for ImageNet-C. Compared with MAE models, GPaco enjoys better generalization ability and stronger robustness on ImageNet and its variants.

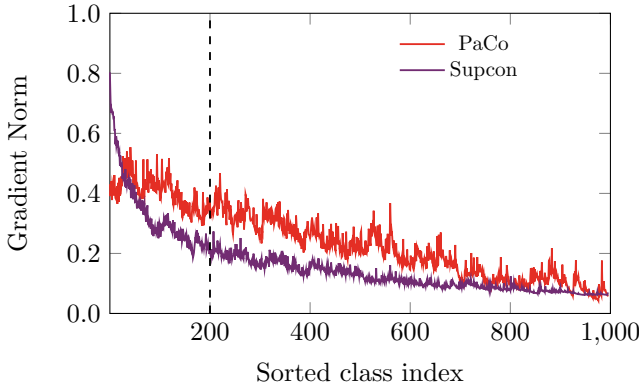


Fig. 2. **Rebalance in contrastive learning.** We collect the average L2 norm of the gradient of weights in the last classifier layer on ImageNet-LT. Category indices are sorted by their image counts. The gradient norm varying from the most frequent class to the least one is steep for supervised contrastive learning [20]. In particular, the gradient norm dramatically decreases for the top 200 most frequent classes. Trained with PaCo, the gradient norm is better balanced.

effects of each component in PaCo including augmentation strategy, loss function (relation to multi-task), momentum encoder and queue size. Simplifying it to **Generalized Parametric Contrastive Learning (GPaco)** by removing the momentum encoder boosts model performance and robustness. Moreover, GPaco demonstrates its great generality with various tasks in Fig 1.

Finally, we conduct experiments on imbalanced data including long-tailed version of CIFAR [35], [36], ImageNet [37], Places [37] and iNaturalist 2018 [38]. Experimental results show that we create a new record for long-tailed recognition. On balanced data, We testify the effectiveness of GPaco on full ImageNet [11] and CIFAR [39]. Compared with MAE models, we achieve better generalization ability and stronger robustness. With GPaco loss for semantic segmentation, obvious improvements are obtained on popular benchmarks including ADE20K [40], COCO-Stuff

[41], PASCAL Context [42] and Cityscapes [43]. Our key contributions are as follows.

- We identify the shortcoming of supervised contrastive learning under an imbalanced setting – it tends to bias high-frequency classes.
- We extend supervised contrastive loss to the PaCo loss, which is more friendly to imbalanced learning, by introducing a set of parametric class-wise learnable centers.
- We examine the necessary of components in PaCo and simplify PaCo to GPaco, observing that the momentum encoder can hurt model performance and should be removed.
- GPaco can benefit the training on imbalanced data and balanced data varying from CNNs to vision transformers. Experiments on tasks *e.g.*, long-tailed classification, full ImageNet/CIFAR classification, out-of-distribution robustness, and semantic segmentation demonstrate the generality of GPaco.

2 RELATED WORK

Re-sampling/re-weighting. The most classical way to deal with long-tailed datasets is to over-sample low-frequency class images [26], [44], [45], [46] or under-sample high-frequency class images [24], [45], [47]. However, Oversampling can suffer from heavy over-fitting to low-frequency classes especially on small datasets. For under-sampling, discarding a large portion of high-frequency class data inevitably causes degradation of the generalization ability of CNNs. Re-weighting [48], [49], [50], [51], [52], [53] the loss functions is an alternative way to rebalance by either enlarging weights on more challenging and sparse classes or randomly ignoring gradients from high-frequency classes [54]. However, with large-scale data, re-weighting makes CNNs difficult to optimize during training [48], [49].

One/two-stage Methods. Since deferred re-weighting and re-sampling were proposed by Cao [36], Kang [28] and

Zhou [55] observed re-weighting or re-sampling strategies could benefit classifier learning while hurting representation learning. Kang [28] proposed to decompose representation and classifier learning. It first trains the CNNs with uniform sampling, and then fine-tune the classifier with class-balanced sampling while keeping parameters of representation learning fixed. Zhou [55] proposed one cumulative learning strategy, with which they bridge representation learning and classifier re-balancing.

The two-stage design is not for end-to-end frameworks. Tang [31] analyzed the reason from the perspective of causal graph and concluded that the bad momentum causal effects played a vital role. Cui [30] proposed residual learning mechanism to address this issue.

Non-parametric Contrastive Loss. Contrastive learning [15], [16], [17], [18], [19] is a framework that learns similar/dissimilar representations from data that are organized into similar/dissimilar pairs. An effective contrastive loss function, called InfoNCE [56], is

$$\mathcal{L}_{q,k^+,\{k^-\}} = -\log \frac{\exp(q \cdot k^+ / \tau)}{\exp(q \cdot k^+ / \tau) + \sum_{k^-} \exp(q \cdot k^- / \tau)}, \quad (1)$$

where q is a query representation, k^+ is for the positive (similar) key sample, and $\{k^-\}$ denotes negative (dissimilar) key samples. τ is a temperature hyper-parameter. In the instance discrimination pretext task [57] for self-supervised learning, a query and a key form a positive pair if they are data-augmented versions of the same image. It forms a negative pair otherwise.

Traditional cross-entropy with linear fc layer weight w and true label y among n classes is expressed as

$$\mathcal{L}_{cross-entropy} = -\log \frac{\exp(q \cdot w_y)}{\sum_{i=1}^n \exp(q \cdot w_i)}. \quad (2)$$

Compared to it, InfoNCE does not get involved with parametric learnable parameters. To distinguish our proposed parametric contrastive learning from previous ones, we treat the InfoNCE as a non-parametric contrastive loss following [58].

Chen [15] used self-supervised contrastive learning SimCLR to first match the performance of a supervised ResNet-50 with only a linear classifier trained on self-supervised representation on full ImageNet. He [16] proposed MoCo and Chen [17] extended MoCo to MoCo v2, with which small batch size training can also achieve competitive results on full ImageNet [11]. In addition, many other methods [18], [19] are also proposed to further boost performance.

3 PARAMETRIC CONTRASTIVE LEARNING

3.1 Supervised Contrastive Learning

Khosla [20] extended the self-supervised contrastive loss with label information into supervised contrastive loss. Here we present it in the framework of MoCo [16], [17] as

$$\mathcal{L}_i = - \sum_{z_+ \in P(i)} \log \frac{\exp(z_+ \cdot T(x_i))}{\sum_{z_k \in A(i)} \exp(z_k \cdot T(x_i))}. \quad (3)$$

MoCo framework [16], [17] consists of two networks with the same structure, *i.e.*, *query network* and *key network*. The

TABLE 1
Supervised contrastive learning is more sensitive to data imbalance. Top-1 accuracy (%) on ImageNet-LT with ResNet-50 is reported. Implementation details are in supplementary file. “+” represents model is trained with PaCo loss without center learning rebalance.

Method	Many	Medium	Few	All
Cross-Entropy	67.5	42.6	13.7	48.4
SupCon	53.4	2.9	0	22.0
PaCo (ours) +	69.6	45.8	16.0	51.0

key network is driven by a momentum update with the query network in training. For each network, it usually contains one encoder CNN and one two-layer MLP transform.

During training, for one two-viewed image batch $B = (B_{v1}, B_{v2})$ and label y , B_{v1} and B_{v2} are fed into the query network and key network respectively and we denote their outputs as Z_{v1} and Z_{v2} . Especially, Z_{v2} is used to update the momentum *queue*.

In Eq. (3), x_i is the representation for image X_i in B_{v1} obtained by the encoder of query network. The transform $T(\cdot)$ also belongs to the query network. We write

$$A(i) = \{z_k \in queue \cup Z_{v1} \cup Z_{v2}\} \setminus \{z_k \in Z_{v1} : k = i\},$$

$$P(i) = \{z_k \in A(i) : y_k = y_i\}.$$

In implementation, the loss is usually scaled by $\frac{1}{|P(i)|}$ and a temperature τ is applied like in Eq. (1). Different from self-supervised contrastive loss, which treats query and key as a positive pair if they are the data-augmented version of the same image, supervised contrastive loss treats them as one positive pair if they belong to the same class.

3.2 Theoretical Motivation

Analysis of Supervised Contrastive Learning. Khosla [20] introduced supervised contrastive learning to encourage more compact representation. We observe that it is not directly applicable to long-tailed recognition. As shown in Table 1, the performance significantly decreases compared with traditional supervised cross-entropy. From an optimization point of view, supervised contrastive loss concentrates more on high-frequency classes than low-frequency ones, which is unfriendly for imbalanced learning.

Remark 1. (Optimal value for supervised contrastive learning). When supervised contrastive loss converges, the optimal value for the probability that two samples are a true positive pair with label y is $\frac{1}{K_y}$, where, $q(y)$ is the frequency of class y over the whole dataset, *queue* is the momentum *queue* in MoCo [16], [17] and $K_y \approx \text{length}(\text{queue}) \cdot q(y)$. *Proof* See supplementary material.

Interpretation. As indicated by Remark 1, high-frequency classes have a higher lower bound of loss value and contribute much more importance than low-frequency classes in training. Thus the training process can be dominated by high-frequency classes. To handle this issue, we introduce a

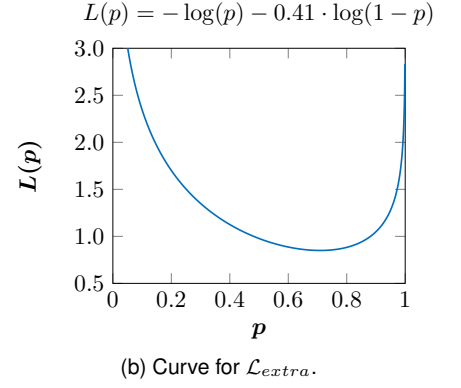
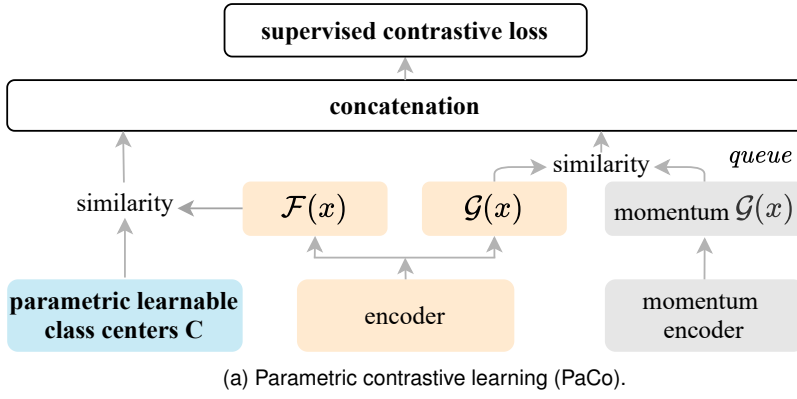


Fig. 3. **Framework of Parametric Contrastive Learning (PaCo) and \mathcal{L}_{extra} curve.** (a) shows the detail of PaCo. We introduce a set of parametric class-wise learnable centers for rebalancing in contrastive learning. More analysis is in Section 3.3 for PaCo. (b) plots the curve of \mathcal{L}_{extra} instantiated with full ImageNet. More analysis on balanced data is in Section 3.4.

set of parametric class-wise learnable centers for rebalancing in contrastive learning.

3.3 Rebalance in Contrastive Learning

As described in Fig. 3 (a), we introduce a set of parametric class-wise learnable centers $\mathbf{C} = \{c_1, c_2, \dots, c_n\}$ into the original supervised contrastive learning, and called this new form **Parametric Contrastive Learning (PaCo)**. Correspondingly, the loss function is changed to

$$\mathcal{L}_i = \sum_{z_+ \in P(i) \cup \{c_y\}} -w(z_+) \log \frac{\exp(z_+ \cdot T(x_i))}{\sum_{z_k \in A(i) \cup \mathbf{C}} \exp(z_k \cdot T(x_i))}, \quad (4)$$

where

$$w(z_+) = \begin{cases} \alpha, & z_+ \in P(i) \\ 1.0, & z_+ \in \{c_y\} \end{cases}$$

and

$$z \cdot T(x_i) = \begin{cases} z \cdot \mathcal{G}(x_i), & z \in A(i) \\ z \cdot \mathcal{F}(x_i), & z \in \mathbf{C}. \end{cases}$$

Following Chen [17], the transform $\mathcal{G}(\cdot)$ is a two-layer MLP while $\mathcal{F}(\cdot)$ is the identity mapping, i.e., $\mathcal{F}(x) = x$. α is one hyper-parameter in (0,1). $P(i)$ and $A(i)$ are the same with supervised contrastive learning in Eq. (3). In implementation, the loss is scaled by $\frac{1}{\sum_{z_+ \in P(i) \cup \{c_y\}} w(z_+)}$ and a temperature τ is applied like in Eq. (3).

Remark 2. (Optimal value for parametric contrastive learning) When parametric contrastive loss converges, the optimal value for the probability that two samples are a true positive pair with label y is $\frac{\alpha}{1 + \alpha \cdot K_y}$ and the optimal value for the probability that a sample is closest to its corresponding center c_y among \mathbf{C} is $\frac{1}{1 + \alpha \cdot K_y}$, where $q(y)$ is the frequency of class y over the whole dataset, $queue$ is the momentum queue in MoCo [16], [17] and $K_y \approx \text{length}(queue) \cdot q(y)$. *Proof* See the Supplementary Material.

Interpretation. Suppose the most frequent class y_h has $K_{y_h} \approx q(y_h) \cdot \text{length}(queue)$ and the least frequent class y_t

has $K_{y_t} \approx q(y_t) \cdot \text{length}(queue)$. As indicated by Remarks 2 and 1, the optimal value for the probability that two samples are a true positive pair varying from the most frequent class to the least one is rebalanced from $\frac{1}{K_{y_h}} \rightarrow \frac{1}{K_{y_t}}$ to $\frac{1}{\frac{1}{\alpha} + K_{y_h}} \rightarrow \frac{1}{\frac{1}{\alpha} + K_{y_t}}$. The smaller α , the more uniform the optimal value from the most frequent class to the least one is, friendly to low-frequency classes learning.

However, when α decreases, the intensity of contrast among samples will be weaker, the intensity of contrast between samples and centers will be stronger. The whole loss becomes closer to supervised cross-entropy. To make good use of contrastive learning and rebalance at the same time, we observe that $\alpha=0.05$ is a reasonable choice.

3.4 PaCo under balanced setting

For balanced datasets, all classes have the same frequency, i.e., $q^* = q(y_i) = q(y_j)$ and $K^* = K_{y_i} = K_{y_j}$ for any class y_i and class y_j . In this case, PaCo reduces to an improved version of multi-task with weighted sum of supervised cross-entropy loss and supervised contrastive loss. The connection between PaCo and multi-task is

$$ExpSum = \sum_{c_k \in \mathbf{C}} \exp(c_k \cdot \mathcal{F}(x_i)) + \sum_{z_k \in A(i)} \exp(z_k \cdot \mathcal{G}(x_i)).$$

We also write the PaCo loss as

$$\begin{aligned} \mathcal{L}_i &= \sum_{z_+ \in P(i) \cup \{c_y\}} -w(z_+) \log \frac{\exp(z_+ \cdot T(x_i))}{\sum_{z_k \in A(i) \cup \mathbf{C}} \exp(z_k \cdot T(x_i))} \\ &= -\log \frac{\exp(c_y \cdot \mathcal{F}(x_i))}{ExpSum} - \alpha \sum_{z_+ \in P(i)} \log \frac{\exp(z_+ \cdot \mathcal{G}(x_i))}{ExpSum} \\ &= \mathcal{L}_{sup} + \alpha \mathcal{L}_{supcon} - (\log P_{sup} + \alpha K^* \log P_{supcon}) \\ &= \mathcal{L}_{sup} + \alpha \mathcal{L}_{supcon} - (\log P_{sup} + \alpha K^* \log(1 - P_{sup})), \end{aligned}$$

$$\text{where} \quad \begin{cases} P_{sup} = \frac{\sum_{c_k \in \mathbf{C}} \exp(c_k \cdot \mathcal{F}(x_i))}{ExpSum}; \\ P_{supcon} = \frac{\sum_{z_k \in A(i)} \exp(z_k \cdot \mathcal{G}(x_i))}{ExpSum}. \end{cases} \quad (5)$$

Multi-task learning combines supervised cross-entropy loss and supervised contrastive loss with a fixed weighted scalar. When these two losses conflict, the training can suffer from slower or sub-optimization. Our PaCo contrarily adjust the intensity of supervised cross-entropy loss and supervised contrastive loss in an adaptive way and potentially avoids conflict as analyzed in the following.

3.4.1 Analysis of PaCo under balanced setting

As indicated by Eq. (5), compared with multi-task, PaCo has an additional loss item:

$$\mathcal{L}_{extra} = -\log(P_{sup}) - \alpha K^* \log(1 - P_{sup}). \quad (6)$$

Here, we take full ImageNet as an example, *i.e.*, $q^* = 0.001$, $\text{length}(\text{queue}) = 8192$, $\alpha = 0.05$, $\alpha K^* = 0.41$. Then the function curve for \mathcal{L}_{extra} is shown in Fig. 3 (b). With P_{sup} increases from 0 to 1.0, the function value decreases until $P_{sup} = 0.71$ and then goes up, which implies \mathcal{L}_{extra} obtains the smallest loss value when $P_{sup} = 0.71$. Note that, when the whole PaCo loss in Eq. (4) achieves the optimal solution, $P_{sup} = 0.71$ still establishes as demonstrated by Remark 2. With P_{sup} increases in the training, we analyze how does it affect the intensity of supervised contrastive loss and supervised cross-entropy loss in the following.

bf Adaptive weighting between \mathcal{L}_{sup} and \mathcal{L}_{supcon} . Note that the optimal value for the probability that two samples are a true positive pair with label y is 0.035 as indicated by Remark 2. We suppose $p_l, p_h \in (0, 0.71)$ and $p_l < p_h$. To achieve the optimal value, when $P_{sup}=p$, the supervised contrastive loss value \mathcal{L}_{supcon} must decrease as in Eq. (7).

$$\begin{aligned} \mathcal{L}_{supcon} &= - \sum_{z_+ \in P(i)} \log \frac{\exp(z_+ \cdot \mathcal{G}(x_i))}{\sum_{z_k \in A(i)} \exp(z_k \cdot \mathcal{G}(x_i))} \\ &= - \sum_{z_+ \in P(i)} \log \frac{\frac{\exp(z_+ \cdot \mathcal{G}(x_i))}{ExpSum}}{\frac{\sum_{z_k \in A(i)} \exp(z_k \cdot \mathcal{G}(x_i))}{ExpSum}} \\ &= - K^* \log \frac{0.035}{1-p}. \end{aligned} \quad (7)$$

Here P_{sup} increases from p_l to p_h , \mathcal{L}_{supcon} must decrease to a much smaller loss value to achieve the optimal solution, which implies the need to make two different class samples much more discriminative, *i.e.*, increasing inter-class margins, and thus the intensity of supervised contrastive loss will enlarge.

An intuition is that as P_{sup} increases, more samples are pulled together with their corresponding centers. Along with stronger intensity of supervised contrastive loss at that time, it is more likely to push hard examples close to those samples that are already around right centers.

3.5 Center Learning Rebalance

PaCo balances the contrastive learning (for moderating contrast among samples). However the center learning also needs to be balanced, which has been explored in [21], [22], [23], [24], [25], [26], [27], [28], [29], [30], [31], [32], [59]. We incorporate Balanced Softmax [27] into the center learning.

Then the PaCo loss is changed from Eq. (4) to what follows:

$$\mathcal{L}_i = \sum_{z_+ \in P(i) \cup \{c_y\}} -w(z_+) \log \frac{\psi(z_+, T(x_i))}{\sum_{z_k \in A(i) \cup \mathbf{C}} \psi(z_k, T(x_i))}, \quad (8)$$

where

$$\psi(z_k, T(x_i)) = \begin{cases} \exp(z_k \cdot \mathcal{G}(x_i)), & z_k \in A(i); \\ \exp(z_k \cdot \mathcal{F}(x_i)) \cdot q(y_k), & z_k \in \mathbf{C}. \end{cases}$$

We emphasize that Balanced Softmax is only a practical remedy for center learning rebalance. The theoretical analysis remains as a future work.

3.6 Generalized Parametric Contrastive Learning

MoCo [16] and MoCo v2 [17] use a momentum encoder and a queue to allow small mini-batch training and achieve even better performance than SimCLR [15] which requires large mini-batch training, in self-supervised learning.

To simplify the framework of PaCo, we validate how each component, *i.e.*, augmentation strategy, formulation of GPaCo/PaCo, the momentum encoder and queue size, make effects in Sec. 4.5. Interestingly, we observe that the derived Generalized Parametric Contrastive Learning (GPaCo) by removing the momentum encoder boosts performance on imbalanced and balanced data again.

In addition to long-tailed recognition, GPaCo models enjoy better generalization ability across CNNs (ResNets) to vision transformers (ViT models) on full ImageNet and CIFAR, which is demonstrated in Sec. 4.2 and Sec. 4.3. Besides image classification, GPaCo shows its great generality on other tasks, *e.g.*, out-of-distribution robustness, and semantic segmentation.

To demonstrate the advantages of GPaCo on out-of-distribution data, we load MAE [14] pre-trained weights and then fine-tune on full ImageNet with same training strategy as in [14]. Compared with MAE baselines, GPaCo models achieve much stronger robustness across different benchmarks, which is discussed in Sec. 4.3.

For semantic segmentation task, GPaCo treats each pixel as an example. However, huge number of pixels make it impractical to directly apply GPaCo to pixel classification. To reduce computational cost and GPU memory, we randomly sample 8192 pixels from down-sampled pixel features. These selected pixel features go through a 3-layer mlp transform and then are fed into GPaCo, which is adopted as an auxiliary loss for training optimization. GPaCo models on semantic segmentation show obvious improvements compared with baselines across 4 most popular datasets in semantic segmentation community. More details are introduced in Sec. 4.4.

4 EXPERIMENTS

4.1 Long-tailed Recognition

We follow the common evaluation protocol [28], [30], [37] in long-tailed recognition – that is, training models on the long-tailed source label distribution and evaluating their performance on the uniform target label distribution. We conduct experiments on long-tailed version of CIFAR-100

TABLE 2

Top-1 accuracy on ImageNet-LT for different backbone architectures. “†” denotes models are trained with RandAugment [60] in 400 epochs. More comparisons with RIDE [29] are in Fig. 1.

Method	ResNet-50	ResNeXt-50	ResNeXt-101
CE(baseline)	41.6	44.4	44.8
Decouple-cRT	47.3	49.6	49.4
Decouple- τ -norm	46.7	49.4	49.6
De-confound-TDE	51.7	51.8	53.3
ResLT	-	52.9	54.1
MiSLAS	52.7	-	-
Decouple- τ -norm †	54.5	56.0	57.9
Balanced Softmax †	55.0	56.2	58.0
PaCo†	57.0	58.2	60.0
GPaCo†	58.5	58.9	60.8

[35], [36], Places [37], ImageNet [37] and iNaturalist 2018 [38] datasets.

CIFAR-100-LT datasets. We use the long-tailed version of CIFAR datasets with the same setting as those used in [35], [55], [61]. They control the degrees of data imbalance with an imbalance factor β . $\beta = \frac{N_{max}}{N_{min}}$ where N_{max} and N_{min} are the numbers of training samples for the most and least frequent classes respectively. Following [55], we conduct experiments with imbalance factors 100, 50, and 10.

ImageNet-LT and Places-LT. ImageNet-LT and Places-LT were proposed in [37]. ImageNet-LT is a long-tailed version of ImageNet dataset [11] by sampling a subset following the Pareto distribution with power value $\alpha=6$. It contains 115.8K images from 1,000 categories, with class cardinality ranging from 5 to 1,280. Places-LT is a long-tailed version of the large-scale scene classification dataset Places [13]. It consists of 184.5K images from 365 categories with class cardinality ranging from 5 to 4,980.

iNaturalist 2018. The iNaturalist 2018 [38] is one species classification dataset, which is on a large scale and suffers from extremely imbalanced label distribution. It is composed of 437.5K images from 8,142 categories. In addition to the extreme imbalance, the iNaturalist 2018 dataset also confronts the fine-grained problem [62].

Implementation details. For image classification on ImageNet-LT, we used ResNet-50, ResNeXt-50-32x4d, and ResNeXt-101-32x4d as our backbones for experiments. For iNaturalist 2018, we conduct experiments with ResNet-50 and ResNet-152. All models were trained using SGD optimizer with momentum $\mu = 0.9$.

Contrastive learning benefits from longer training compared with traditional supervised learning with cross-entropy as Chen [15] concluded, which is also validated by previous work of [15], [16], [17], [18], [19]. MoCo [16], [17], BYOL [18] and SWAV [19] train 800 epochs for model convergence. Supervised contrastive learning [20] trains 350 epochs for feature learning and another 350 epochs for classifier learning.

Following MoCo [16], [17], when we train models with GPaCo/PaCo, the learning rate decays by a cosine scheduler from 0.04/0.02 to 0 with batch size 128 on 4 GPUs in 400 epochs. The temperature is set to 0.2. α is 0.05. For a fair comparison, we re-implement baselines with the same

TABLE 3

Performance on Places-LT [37], starting from an ImageNet pre-trained ResNet-152 provided by torchvision. “†” denotes the model trained with RandAugment [60].

Method	Many	Medium	Few	All
CE(baseline)	45.7	27.3	8.2	30.2
OLTR	44.7	37.0	25.3	35.9
Decouple- τ -norm	37.8	40.7	31.8	37.9
Balanced Softmax	42.0	39.3	30.5	38.6
ResLT	39.8	43.6	31.4	39.8
MiSLAS	39.6	43.3	36.1	40.4
RIDE (2 experts)	-	-	-	-
PaCo	37.5	47.2	33.9	41.2
PaCo †	36.1	47.9	35.3	41.2
GPaCo	39.5	47.2	33.0	41.7

training time and RandAugment [60] for recent state-of-the-arts of Decouple [28], Balanced Softmax [27] and RIDE [29]. Especially, for RIDE, based on model ensemble, we compare with it under comparable inference latency in Fig. 1 (a).

For Places-LT, following previous setting [30], [37], we choose ResNet-152 as the backbone network, pre-train it on the full ImageNet-2012 dataset (provided by torchvision), and finely tune it for 30 epochs on Places-LT. The learning rate decays by a cosine scheduler from 0.02 to 0 with batch size 128. The temperature is set to 0.2. α is 0.02/0.05 for GPaCo and PaCo. For CIFAR-100-LT, we strictly follow the setting of [27] for fair comparison. A smaller temperature of 0.07 and $\alpha = 0.01$ are adopted.

Comparison on ImageNet-LT. Table 2 shows extensive experimental results for comparison with recent SOTA methods. We observe that Balanced Softmax [27] still achieves comparable results with Decouple [28] across various backbones under such strong training setting on ImageNet-LT, consistent with what is claimed in the original paper. For RIDE that is based on model ensemble, we analyze the real inference speed by calculating inference time with a batch of 64 images on Nvidia GeForce 2080Ti GPU.

We observe RIDEResNet with 3 experts even has higher inference latency than a standard ResNeXt-50-32x4d (**15.3ms vs 13.1ms**); RIDEResNeXt with 3 experts yields higher inference latency than a standard ResNeXt-101-32x4d (**26ms vs 25ms**). This result is in accordance with the conclusion that network fragmentation reduces the degree of parallelism and thus decreases efficiency in [9], [63]. For fair comparison, we do not apply knowledge distillation tricks for all these methods. As shown in Fig. 1 (a) and Table 2, under comparable inference latency, GPaCo/PaCo significantly surpasses these baselines.

Comparison on Places-LT. The experimental results on Places-LT are summarized in Table 3. Due to the architecture change of RIDE, it is not applicable to load the publicly pre-trained model on full ImageNet, while GPaCo/PaCo is more flexible because the network architecture is the same as those of [30], [37]. Under fair training setting by finely tuning 30 epochs without RandAugment, PaCo surpasses SOTA Balanced Softmax by 2.6%. GPaCo even achieves 41.7% after removing the momentum encoder. An interesting observation is that RandAugment has little effect on the Places-LT dataset. A similar phenomenon can be

TABLE 4

Evaluation with ViT models [64] on full ImageNet and out-of-distribution data. GPaCo models enjoy better generalization ability and stronger robustness compared with MAE models. We use their official open-source code for reproducing results of MAE models with 8 Nvidia GeForce RTX3090 GPUs. Top-1 accuracy are reported for full ImageNet, ImageNet-R, and ImageNet-S. mCE and rel. mCE are reported for ImageNet-C.

Method	Model	Full ImageNet (\uparrow)	ImageNet-C (mCE \downarrow)	ImageNet-C (rel. mCE \downarrow)	ImageNet-R (\uparrow)	ImageNet-S (\uparrow)
w/ Mixup and CutMix						
MAE	ViT-B	83.6	39.1	49.9	49.9	36.1
MAE	ViT-L	85.7	32.4	41.4	60.3	45.5
w/o Mixup and CutMix						
SupCon	ResNet-50	78.7	67.2	94.6	-	-
GPaCo	ResNet-50	79.7	50.9	64.4	41.1	30.9
MAE	ViT-B	82.5	44.9	56.9	44.9	32.9
MAE	ViT-L	85.2	36.4	46.3	55.3	42.6
GPaCo	ViT-B	84.0	37.2	47.3	51.7	39.4
GPaCo	ViT-L	86.0	30.7	39.0	60.3	48.3

TABLE 5

Top-1 accuracy on full ImageNet with ResNets. “*” denotes supervised contrastive learning with additional operation of image warping before Gaussian blur.

Method	Model	augmentation	Top-1 Acc
Supcon	ResNet-50	SimAugment *	77.9
Supcon	ResNet-50	RandAugment	78.4
Supcon	ResNet-101	StackedRandAugment	80.2
multi-task	RandAugment	ResNet-50	78.1
PaCo	ResNet-50	SimAugment	78.7
PaCo	ResNet-50	RandAugment	79.3
PaCo	ResNet-101	StackedRandAugment	80.9
PaCo	ResNet-200	StackedRandAugment	81.8
GPaCo	ResNet-50	RandAugment	79.5
GPaCo	ResNet-50	StackedRandAugment	79.7

observed on the iNaturalist 2018 dataset. More evaluation numbers are in the supplementary file. They can be intuitively understood since RandAugment is designed for ImageNet classification, which inspires us to explore general augmentations across different domains.

Comparison on iNaturalist 2018. Table 6 lists experimental results on iNaturalist 2018. Under fair training setting, PaCo consistently surpasses recent SOTA methods of Decouple, Balanced Softmax and RIDE. Our method is 1.4% higher than Balanced Softmax. We also apply PaCo on large ResNet-152 architecture. And the performance boosts to **75.3%** top-1 accuracy. Surprisingly, With GPaCo, a ResNet-50 model achieves **75.4%** top-1 accuracy, implying that the momentum encoder for PaCo can hurt optimization in training. Note that we only transfer the hyper-parameters of PaCo on ImageNet-LT to iNaturalist 2018 without any change. Tuning hyper-parameters for GPaCo/PaCo will bring further improvement.

Comparison on CIFAR-100-LT. The experimental results on CIFAR-100-LT are listed in Table 8. For the CIFAR-100-LT dataset, we mainly compare with the SOTA method Balanced Softmax [27] with the same training setting where Cutout [65] and AutoAugment [66] are used in training. As shown in Table 8, PaCo consistently outperforms Balanced Softmax across different imbalance factors with such

TABLE 6

Top-1 accuracy over all classes on iNaturalist 2018 with ResNet-50. Knowledge distillation is not applied for fair comparison. We compare with RIDE under comparable inference latency. “†” denotes models trained with RandAugment [60] in 400 epochs.

Method	Top-1 Acc
LDAM+DRW	68.0
Decouple-LWS	69.5
BBN	69.6
ResLT	70.2
MiSLAS	71.6
RIDE (2 experts) †	69.5
Decouple- τ -norm †	71.5
Balanced Softmax †	71.8
PaCo †	73.2
GPaCo †	75.4

a strong setting. Specifically, PaCo surpasses Balanced Softmax by 1.2%, 1.8% and 1.2% under imbalance factor 100, 50 and 10 respectively, which testify the effectiveness of our PaCo method. GPaCo models show better performance than PaCo models.

4.2 Full ImageNet and CIFAR Recognition

As analyzed in Section 3.4, for balanced datasets, PaCo reduces to an improved version of multi-task learning, which adaptively adjusts the intensity of supervised cross-entropy loss and supervised contrastive loss. To verify the effectiveness of PaCo under this balanced setting, we conduct experiments on full ImageNet and full CIFAR. They are indicative to compare GPaCo/PaCo with supervised contrastive learning (Supcon) [20]. Note that, under full ImageNet and CIFAR, we remove the rebalance in center learning, *i.e.*, Balanced Softmax, for fair comparisons.

Full ImageNet. In the implementation, we transfer hyper-parameters of GPaCo/PaCo on ImageNet-LT to full ImageNet without modification. SGD optimizer with momentum $\mu = 0.9$ is used. $\alpha=0.05$, temperature is 0.2 and queue size is 8,192. For multi-task training, the supervised contrastive loss is an additional regularization and the loss weight is extensively explored from 0.1 to 1.0 in Sec.

TABLE 7
Transferring GPaCo to the semantic segmentation.

Method	Backbone	mIoU (s.s.)	mIoU (m.s.)
ADE20K Dataset			
UperNet	Swin-T	44.5	45.8
	Swin-B	50.0	51.7
	Swin-L	52.0	53.5
UperNet w/ GPaCo	Swin-T	45.4	46.8
	Swin-B	51.6	53.2
	Swin-L	52.8	54.3
COCO-Stuff Dataset			
deeplabv3+	ResNet-50	35.8	36.8
	ResNet-101	38.1	39.0
deeplabv3+ w/ GPaCo	ResNet-50	37.0	37.9
	ResNet-101	38.8	40.1
PASCAL Context Dataset			
deeplabv3+	ResNet-50	50.5	52.1
	ResNet-101	52.9	54.5
deeplabv3+ w/ GPaCo	ResNet-50	51.9	53.7
	ResNet-101	54.2	56.2
Cityscapes			
deeplabv3+	ResNet-18	76.9	78.8
	ResNet-50	80.1	81.1
	ResNet-101	81.0	82.0
deeplabv3+ w/ GPaCo	ResNet-18	78.1	79.7
	ResNet-50	80.8	82.0
	ResNet-101	81.4	82.1

4.5. The same data augmentation strategy is applied as in GPaCo/PaCo, which is discussed in Section 4.5.

The experimental results are summarized in Table 5. With SimAugment, our ResNet-50 PaCo model achieves 78.7% top-1 accuracy, which outperforms supervised contrastive learning model by 0.8%. Equipped with strong augmentation, *i.e.*, RandAugment [60], the performance further improves to 79.3%. ResNet-101/200 trained with PaCo consistently surpass supervised contrastive learning. Replacing PaCo with GPaCo, The ResNet-50 model boosts to **79.7%** top-1 accuracy.

Full CIFAR-100. For CIFAR implementation, we follow supervised contrastive learning and train ResNet-50 with only the SimAugment. Compared with full ImageNet, we adopt a smaller temperature of 0.07, $\alpha = 0.01$ and batch size 256 with learning rate 0.1. As shown in Table 9, on CIFAR-100, PaCo outperforms supervised contrastive learning by 2.6%, which validates the advantages of PaCo. Again, the GPaCo model achieves **80.3%** top-1 accuracy, significantly surpassing supervised contrastive learning by 3.8%. Note that, following [9], we use a weight-decay of 5e-4.

4.3 Out-of-distribution Robustness

He et al. [14] justifies that masked autoencoders are scalable vision learners. With such a simple pre-training strategy that masking random patches of the input image and reconstructing the missing pixels, the good representation is learned and well transferred to downstream tasks, *i.e.*, full ImageNet classification, object detection, semantic segmentation, and robustness on out-of-distribution data. In this

TABLE 8
Top-1 accuracy on CIFAR-100-LT with different imbalance factors. “†” represents that models are trained in same setting.

Dataset	CIFAR-100 LT		
Imbalance factor	100	50	10
Focal Loss	38.4	44.3	55.8
LDAM+DRW	42.0	46.6	58.7
BBN	42.6	47.0	59.1
Causal Norm	44.1	50.3	59.6
ResLT	45.3	50.0	60.8
MiSLAS	47.0	52.3	63.2
Balanced Softmax †	50.8	54.2	63.0
PaCo †	52.0	56.0	64.2
GPaCo †	52.3	56.4	65.4

TABLE 9
Top-1 accuracy on full CIFAR-100 with ResNet-50.

Method	dataset	Top-1 Acc
CE(baseline)	CIFAR-100	77.9
multi-task	CIFAR-100	78.0
Supcon	CIFAR-100	76.5
PaCo	CIFAR-100	79.1
GPaCo	CIFAR-100	80.3

section, we verify that GPaCo can enhance model generalization ability and robustness on full ImageNet and its variants when compared with MAE [14] models.

Robustness Evaluation. We extensively evaluate the model performance on out-of-distribution robustness using following benchmarks: 1) ImageNet-C [67], with various common image corruptions; 2) ImageNet-R [68], which contains natural renditions of ImageNet object classes with different textures and local image statistics; 3) ImageNet-Sketch [69], which includes sketch images of the same ImageNet classes collected online.

Comparison with MAE Models [14]. We summarize experimental results in Table 4. Top-1 accuracy is reported on full ImageNet, ImageNet-R, and ImageNet-S. Mean Corruption Error (mCE) and Relative Mean Corruption Error (rel. mCE) [67] are used for ImageNet-C. mCE is to measure absolute robustness to corruptions while rel. mCE is a better metric when we compare models with different top-1 accuracy.

Compared with MAE models, we achieve better performance on full ImageNet, surpassing them by **0.4** and **0.3** respectively for ViT-B [64] and ViT-L [64]. On ImageNet-C, ImageNet-R, and ImageNet-S, GPaCo models usually outperforms MAE models by **1.7** ~ **3.3**, demonstrating much stronger robustness on out-of-distribution data.

4.4 Semantic Segmentation

In this section, we transfer GPaCo to the downstream task, *i.e.*, semantic segmentation. In implementation, we use GPaCo as an auxiliary loss. Specifically, for each image, we randomly sample 8192 pixel features on the down-sampled feature map and feed them into GPaCo loss for training optimization.

TABLE 10
Ablation on augmentation strategies for GPaCo/PaCo on ImageNet-LT with ResNet-50.

Methods	View-1	View-2	Top-1 Acc
PaCo	SimAug	SimAug	55.0
PaCo	RandAug	SimAug	57.0
PaCo	RandAug	RandAug	56.5
GPaCo	RandAug	SimAug	57.9
GPaCo	RandAug	RandAugStack	58.5

TABLE 11
Comparison with multi-task re-weighting baselines on ImageNet-LT with ResNet-50. The re-weighting strategy is applied to the supervised contrastive loss. Models are all trained without RandAugment.

Method	Top-1 Acc
CE	48.4
multi-task (CE+Re-weighting)	49.0
multi-task (CE+BalSfx)	48.6
PaCo	51.0

Datasets. ADE20K [40] contains 22K densely annotated images with 150 fine-grained semantic concepts. The training and validation sets consist of 20K and 2K images, respectively. COCO-Stuff [41] includes 10K images from the COCO training set. The training and validation sets consist of 9K and 1K images, respectively. It covers 171 classes. For PASCAL Context [42], the subset of 59 frequent classes is used following previous work. Cityscapes [43] consists of 19 classes, covering street scenes from 50 different cities.

Training and Evaluation. We implement our GPaCo in mmseg codebase [70]. On ADE20K [40], we follow [71] to experiment with Swin transformers and UperNet [72]. On COCO-Stuff [41], Pascal Context [42] and Cityscapes [43], we use ResNet-50/101 and deeplabv3+. Default training hyper-parameters in baselines are adopted in the GPaCo model training phase, *i.e.*, the standard random scale jittering between 0.5 and 2.0, random horizontal flipping, random cropping, as well as random color jittering. We report both single scale (s.s.) and multi-scale (m.s.) evaluation results on validation data. For multi-scale inference, scales of 0.5, 0.75, 1.0, 1.25, 1.5, 1.75 are used.

Results. Experimental results are summarized in Table 7. On ADE20K, obvious improvements are observed from Swin-T to Swin-L models when equipped with GPaCo, outperforming baselines by **1.0, 1.5, 0.8** mIoU respectively. On COCO-Stuff and PASCAL Context, GPaCo models significantly surpass baselines by around **1.1 ~ 1.7** mIoU.

4.5 Ablation Study

Data augmentation strategy for PaCo & GPaCo. Data augmentation is the key for success of contrastive learning as indicated by Chen [15]. For PaCo & GPaCo, we also conduct ablation studies for different augmentation strategies. Several observations are intriguingly different from those of [73]. We experiment with the following ways of data augmentation.

TABLE 12
Comparison with multi-task re-weighting baselines that perform center learning rebalance on ImageNet-LT. Models are all trained with RandAugment in 400 epochs.

Method	Backbone	Weight	Top-1 Acc
multi-task (BalSfx + rw)	ResNeXt-50	0.05	57.0
multi-task (BalSfx + rw)	ResNeXt-50	0.10	57.1
multi-task (BalSfx + rw)	ResNeXt-50	0.20	57.1
multi-task (BalSfx + rw)	ResNeXt-50	0.30	57.0
multi-task (BalSfx + rw)	ResNeXt-50	0.50	57.2
multi-task (BalSfx + rw)	ResNeXt-50	0.80	57.2
multi-task (BalSfx + rw)	ResNeXt-50	1.00	56.9
PaCo	ResNeXt-50	-	58.2
multi-task* (BalSfx + rw)	ResNeXt-50	0.50	58.3
multi-task* (BalSfx + rw)	ResNeXt-50	0.80	58.2
GPaCo	ResNeXt-50	-	58.9
multi-task* (BalSfx + rw)	ResNet-50	0.50	57.8
GPaCo	ResNet-50	-	58.5
multi-task* (BalSfx + rw)	ResNeXt-101	0.50	60.0
GPaCo	ResNeXt-101	-	60.8

TABLE 13
Comparison with multi-task baselines on balanced data.

Method	Backbone	Weight	Top-1 Acc
Full CIFAR-100 Dataset			
multi-task (CE + Supcon)	ResNet-50	0.50	78.0
PaCo	ResNet-50	-	79.1
multi-task* (CE + Supcon)	ResNet-50	0.10	79.0
multi-task* (CE + Supcon)	ResNet-50	0.30	79.1
multi-task* (CE + Supcon)	ResNet-50	0.50	79.1
multi-task* (CE + Supcon)	ResNet-50	0.80	78.9
multi-task* (CE + Supcon)	ResNet-50	1.00	79.0
GPaCo	ResNet-50	-	80.3
Full ImageNet Dataset			
multi-task* (CE + Supcon)	ViT-B	0.50	83.4
GPaCo	ViT-B	-	84.0

- **SimAug:** an augmentation policy [16], [17] that applies random flips and color jitters followed by Gaussian blur.
- **RandAug [60]:** A two stage augmentation policy that uses random parameters in place of parameters tuned by AutoAugment. The random parameters do not need to be tuned and hence reduces the search space.
- **RandAugStack:** RandAug followed by Gaussian blur.

For the common *random resized crop* used along with the above three strategies, work of [73] explains that the optimal hyper-parameter for random resized crop is (0.2,1) in self-supervised contrastive learning. This setting is also adopted by other work of [15], [16], [17], [18], [19]. However, in this paper, we observe severe performance degradation on ImageNet-LT with ResNet-50 (55.0% vs 52.2%) for PaCo when we change the hyper-parameter from (0.08,1) to (0.2, 1). This is because PaCo involves center learning while other self-supervised frameworks only apply non-parametric contrastive loss as described in Section 2. Note that the same phenomenon is also observed on traditional supervised learning with cross-entropy loss.

Another observation is that GPaCo can make better use

TABLE 14
Ablation for the necessary of two-view training on full ImageNet with ViT-B.

Method	Full ImageNet(\uparrow)	ImageNet-C(rel. mCE \downarrow)
single-view	82.5	49.1
two-view	84.0	47.3

TABLE 15
Ablation for model ensemble on ImageNet-LT. “+” represents the ensemble model of a ResNeXt-50 and a ResNeXt-101. “*” represents the results are from their original paper [75].

Method	Many	Medium	Few	All
Single Model				
ResLT*(ResNeXt-50)	63.0	50.5	35.5	52.9
RIDE (ResNeXt-50)	67.2	49.0	28.1	53.2
GPaco (ResNeXt-50)	67.4	57.1	41.2	58.9
GPaco (ResNeXt-101)	68.7	59.5	42.8	60.8
Model Ensemble				
ResLT*	64.0	56.6	44.8	57.6
RIDE	71.8	53.9	32.0	57.8
GPaco (ResNeXt-50 2-experts)	69.9	59.5	43.4	61.3
GPaco +	70.1	61.2	45.0	62.4
GPaco (ResNeXt-101 2-experts)	70.9	62.0	45.2	63.2

of strong augmentations compared with PaCo. The work of [74] demonstrates that directly applying strong data augmentation in MoCo [16], [17] does not work well. Here we observe a similar conclusion with RandAug [60] for PaCo. However, after removing the momentum encoder, GPaco can achieve better performance with stronger augmentation as shown in Table 10.

Multi-task Learning. Re-weighting is a classical method for dealing with imbalanced data. Here we directly apply the re-weighting method of Cui [35] in contrastive learning to compare with PaCo. Moreover, Balanced softmax (BalSfx) [27], as one state-of-the-art method for traditional cross-entropy in long-tailed recognition, is also applied to contrastive learning rebalance. The experimental results are summarized in Table 11. It is obvious PaCo significantly surpasses the two baselines.

PaCo/GPaCo balances the contrastive learning (for moderating contrast among samples). However the center learning also needs to be balanced, which has been explored in [21], [22], [23], [24], [25], [26], [27], [28], [29], [30], [31], [59]. To compare with state-of-the-art methods in long-tailed recognition, we incorporate Balanced Softmax (BalSfx) [27] into the center learning. As shown in Table 12, after rebalance in center learning, GPaco boosts performance to 58.9%, surpassing baselines.

We also verify the advantage of GPaco over multi-task learning on balanced data — full ImageNet and full CIFAR-100. As shown in Table 13, extensive values for the weight between cross-entropy and supervised contrastive learning have been explored. GPaco obviously achieve much higher performance.

GPaco with Queue Length. The queue is designed to enlarge the number of samples for GPaco/PaCo loss. We examine the effects of different queue size on model performance. Empirical study on ImageNet-LT with ResNeXt-50 is

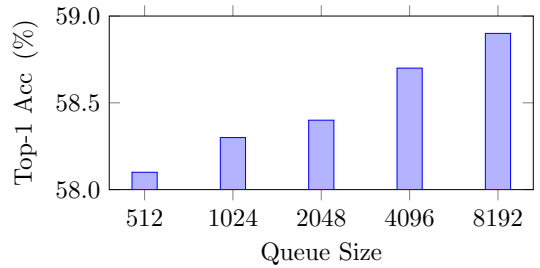


Fig. 4. **The larger queue size, the better performance.** Experimental results with ResNeXt-50 on ImageNet-LT are plotted.

conducted. As shown in Fig 4, the larger queue size usually leads to better performance. However, when the queue size increase from 4096 to 8192, the performance gains become much smaller.

Necessary of Two Views in GPaco. In training of GPaco, a positive pair consists of two images belonging to the same class. We explore whether it is necessary to generate two views as in the self-supervised learning [15], [16], [17]. As shown in Table 14, performance and robustness significantly drops with single view training, which implies the vast importance of two views training in GPaco.

Model Ensemble. Models trained on imbalanced data can easily suffer from over-fitting issue on low-frequency classes, thus leading to high variance of model predictions. RIDE proposes an improved version of model ensemble strategy and has verified the advantages of model ensemble for long-tailed recognition. However, GPaco/PaCo improves single model performance with better feature representation. We go deeper to explore the model ensemble strategy on GPaco models. As shown in Table 15, the improvements coming from model ensemble is much smaller for GPaco models when compared with RIDE and ResLT (improvements of ResLT v.s. RIDE v.s. GPaco are 4.7% v.s. 4.6% v.s. 2.4%), demonstrating that GPaco training can reduce prediction variance of trained models.

5 CONCLUSION

In this paper, we have proposed the Generalized Parametric Contrastive Learning (GPaco/PaCo), which can deal with both imbalanced and balanced data well. It is based on the theoretical analysis of supervised contrastive learning and rebalance from the convergent optimal values. On balanced data, our analysis of PaCo demonstrates that it can adaptively enhance the intensity of pushing two samples of the same class close as more samples are pulled together with their corresponding centers, which can potentially benefit hard examples learning in training.

We conduct experiments on various benchmarks of CIFAR-LT, ImageNet-LT, Places-LT, and iNaturalist 2018. The experimental results show that we create a new state-of-the-art for long-tailed recognition. With balanced data, experimental results on full ImageNet and CIFAR show that GPaco models have better generalization ability and stronger robustness. Transferring GPaco to semantic segmentation, obvious improvements are obtained.

REFERENCES

- [1] K. He, X. Zhang, S. Ren, and J. Sun, "Deep residual learning for image recognition," in *CVPR*, 2016.
- [2] K. Simonyan and A. Zisserman, "Very deep convolutional networks for large-scale image recognition," in *ICLR*, 2015.
- [3] T. Lin, P. Dollár, R. B. Girshick, K. He, B. Hariharan, and S. J. Belongie, "Feature pyramid networks for object detection," in *CVPR*, 2017.
- [4] S. Liu, L. Qi, H. Qin, J. Shi, and J. Jia, "Path aggregation network for instance segmentation," in *CVPR*, 2018.
- [5] H. Zhao, J. Shi, X. Qi, X. Wang, and J. Jia, "Pyramid scene parsing network," in *CVPR*, 2017.
- [6] B. Zoph, V. Vasudevan, J. Shlens, and Q. V. Le, "Learning transferable architectures for scalable image recognition," in *CVPR*, 2018.
- [7] H. Liu, K. Simonyan, and Y. Yang, "DARTS: differentiable architecture search," in *ICLR*. OpenReview.net, 2019.
- [8] M. Tan, B. Chen, R. Pang, V. Vasudevan, M. Sandler, A. Howard, and Q. V. Le, "Mnasnet: Platform-aware neural architecture search for mobile," in *CVPR*, 2019.
- [9] J. Cui, P. Chen, R. Li, S. Liu, X. Shen, and J. Jia, "Fast and practical neural architecture search," in *ICCV*, 2019.
- [10] H. Cai, C. Gan, T. Wang, Z. Zhang, and S. Han, "Once-for-all: Train one network and specialize it for efficient deployment," in *ICLR*, 2020.
- [11] O. Russakovsky, J. Deng, H. Su, J. Krause, S. Satheesh, S. Ma, Z. Huang, A. Karpathy, A. Khosla, and M. Bernstein, "ImageNet large scale visual recognition challenge," *IJCV*, 2015.
- [12] T.-Y. Lin, M. Maire, S. Belongie, J. Hays, P. Perona, D. Ramanan, P. Dollár, and C. L. Zitnick, "Microsoft COCO: Common objects in context," in *ECCV*, 2014.
- [13] B. Zhou, A. Lapedriza, A. Khosla, A. Oliva, and A. Torralba, "Places: A 10 million image database for scene recognition," *IEEE TPAMI*, 2018.
- [14] K. He, X. Chen, S. Xie, Y. Li, P. Dollár, and R. Girshick, "Masked autoencoders are scalable vision learners," in *CVPR*, 2022, pp. 16 000–16 009.
- [15] T. Chen, S. Kornblith, M. Norouzi, and G. E. Hinton, "A simple framework for contrastive learning of visual representations," in *ICML*, 2020.
- [16] K. He, H. Fan, Y. Wu, S. Xie, and R. B. Girshick, "Momentum contrast for unsupervised visual representation learning," in *CVPR*, 2020.
- [17] X. Chen, H. Fan, R. B. Girshick, and K. He, "Improved baselines with momentum contrastive learning," *CoRR*, 2020.
- [18] J. Grill, F. Strub, F. Altché, C. Tallec, P. H. Richemond, E. Buchatskaya, C. Doersch, B. Á. Pires, Z. Guo, M. G. Azar, B. Piot, K. Kavukcuoglu, R. Munos, and M. Valko, "Bootstrap your own latent - A new approach to self-supervised learning," in *NeurIPS*, H. Larochelle, M. Ranzato, R. Hadsell, M. Balcan, and H. Lin, Eds., 2020.
- [19] M. Caron, I. Misra, J. Mairal, P. Goyal, P. Bojanowski, and A. Joulin, "Unsupervised learning of visual features by contrasting cluster assignments," in *NeurIPS*, H. Larochelle, M. Ranzato, R. Hadsell, M. Balcan, and H. Lin, Eds., 2020.
- [20] P. Khosla, P. Teterwak, C. Wang, A. Sarna, Y. Tian, P. Isola, A. Maschinot, C. Liu, and D. Krishnan, "Supervised contrastive learning," in *NeurIPS*, H. Larochelle, M. Ranzato, R. Hadsell, M. Balcan, and H. Lin, Eds., 2020.
- [21] M. Buda, A. Maki, and M. A. Mazurowski, "A systematic study of the class imbalance problem in convolutional neural networks," *Neural Networks*, 2018.
- [22] C. Huang, Y. Li, C. C. Loy, and X. Tang, "Learning deep representation for imbalanced classification," in *CVPR*, 2016.
- [23] Y. Cui, M. Jia, T. Lin, Y. Song, and S. J. Belongie, "Class-balanced loss based on effective number of samples," in *CVPR*, 2019.
- [24] H. He and E. A. Garcia, "Learning from imbalanced data," *IEEE TKDE*, 2009.
- [25] N. V. Chawla, K. W. Bowyer, L. O. Hall, and W. P. Kegelmeyer, "SMOTE: Synthetic minority over-sampling technique," *Journal of Artificial Intelligence Research*, 2002.
- [26] L. Shen, Z. Lin, and Q. Huang, "Relay backpropagation for effective learning of deep convolutional neural networks," in *ECCV*, 2016.
- [27] J. Ren, C. Yu, S. Sheng, X. Ma, H. Zhao, S. Yi, and H. Li, "Balanced meta-softmax for long-tailed visual recognition," in *NeurIPS*, H. Larochelle, M. Ranzato, R. Hadsell, M. Balcan, and H. Lin, Eds., 2020.
- [28] B. Kang, S. Xie, M. Rohrbach, Z. Yan, A. Gordo, J. Feng, and Y. Kalantidis, "Decoupling representation and classifier for long-tailed recognition," in *ICLR*, 2020.
- [29] X. Wang, L. Lian, Z. Miao, Z. Liu, and S. X. Yu, "Long-tailed recognition by routing diverse distribution-aware experts," *CoRR*, vol. abs/2010.01809, 2020.
- [30] J. Cui, S. Liu, Z. Tian, Z. Zhong, and J. Jia, "Reslt: Residual learning for long-tailed recognition," *CoRR*, vol. abs/2101.10633, 2021.
- [31] K. Tang, J. Huang, and H. Zhang, "Long-tailed classification by keeping the good and removing the bad momentum causal effect," in *NeurIPS*, H. Larochelle, M. Ranzato, R. Hadsell, M. Balcan, and H. Lin, Eds., 2020.
- [32] Z. Zhong, J. Cui, S. Liu, and J. Jia, "Improving calibration for long-tailed recognition," in *Proceedings of the IEEE/CVF Conference on Computer Vision and Pattern Recognition (CVPR)*, June 2021, pp. 16 489–16 498.
- [33] J. Cui, Y. Yuan, Z. Zhong, Z. Tian, H. Hu, S. Lin, and J. Jia, "Region rebalance for long-tailed semantic segmentation," *arXiv preprint arXiv:2204.01969*, 2022.
- [34] X. Chen and K. He, "Exploring simple siamese representation learning," in *CVPR*, 2021, pp. 15 750–15 758.
- [35] Y. Cui, M. Jia, T.-Y. Lin, Y. Song, and S. Belongie, "Class-balanced loss based on effective number of samples," in *CVPR*, 2019.
- [36] K. Cao, C. Wei, A. Gaidon, N. Aréchiga, and T. Ma, "Learning imbalanced datasets with label-distribution-aware margin loss," in *NeurIPS*, H. M. Wallach, H. Larochelle, A. Beygelzimer, F. d'Alché-Buc, E. B. Fox, and R. Garnett, Eds., 2019.
- [37] Z. Liu, Z. Miao, X. Zhan, J. Wang, B. Gong, and S. X. Yu, "Large-scale long-tailed recognition in an open world," in *CVPR*, 2019.
- [38] G. Van Horn, O. Mac Aodha, Y. Song, Y. Cui, C. Sun, A. Shepard, H. Adam, P. Perona, and S. Belongie, "The iNaturalist species classification and detection dataset," in *CVPR*, 2018.
- [39] A. Krizhevsky, G. Hinton *et al.*, "Learning multiple layers of features from tiny images," 2009.
- [40] B. Zhou, H. Zhao, X. Puig, S. Fidler, A. Barriuso, and A. Torralba, "Scene parsing through ade20k dataset," in *CVPR*, 2017, pp. 633–641.
- [41] H. Caesar, J. Uijlings, and V. Ferrari, "Coco-stuff: Thing and stuff classes in context," in *CVPR*, 2018, pp. 1209–1218.
- [42] R. Mottaghi, X. Chen, X. Liu, N.-G. Cho, S.-W. Lee, S. Fidler, R. Urtasun, and A. Yuille, "The role of context for object detection and semantic segmentation in the wild," in *CVPR*, 2014, pp. 891–898.
- [43] M. Cordts, M. Omran, S. Ramos, T. Rehfeld, M. Enzweiler, R. Benenson, U. Franke, S. Roth, and B. Schiele, "The cityscapes dataset for semantic urban scene understanding," in *CVPR*, 2016, pp. 3213–3223.
- [44] Q. Zhong, C. Li, Y. Zhang, H. Sun, S. Yang, D. Xie, and S. Pu, "Towards good practices for recognition & detection," in *CVPR workshops*, 2016.
- [45] M. Buda, A. Maki, and M. A. Mazurowski, "A systematic study of the class imbalance problem in convolutional neural networks," *Neural Networks*, 2018.
- [46] J. Byrd and Z. Lipton, "What is the effect of importance weighting in deep learning?" in *ICML*, 2019.
- [47] N. Japkowicz and S. Stephen, "The class imbalance problem: A systematic study," *Intelligent Data Analysis*, 2002.
- [48] C. Huang, Y. Li, C. Change Loy, and X. Tang, "Learning deep representation for imbalanced classification," in *CVPR*, 2016.
- [49] C. Huang, Y. Li, C. L. Chen, and X. Tang, "Deep imbalanced learning for face recognition and attribute prediction," *IEEE TPAMI*, 2019.
- [50] Y.-X. Wang, D. Ramanan, and M. Hebert, "Learning to model the tail," in *NeurIPS*, 2017.
- [51] M. Ren, W. Zeng, B. Yang, and R. Urtasun, "Learning to reweight examples for robust deep learning," in *ICML*, 2018.
- [52] J. Shu, Q. Xie, L. Yi, Q. Zhao, S. Zhou, Z. Xu, and D. Meng, "Meta-weight-net: Learning an explicit mapping for sample weighting," in *NeurIPS*, 2019.
- [53] M. A. Jamal, M. Brown, M.-H. Yang, L. Wang, and B. Gong, "Rethinking class-balanced methods for long-tailed visual recognition from a domain adaptation perspective," in *CVPR*, 2020.
- [54] J. Tan, C. Wang, B. Li, Q. Li, W. Ouyang, C. Yin, and J. Yan, "Equalization loss for long-tailed object recognition," in *CVPR*, 2020.

- [55] B. Zhou, Q. Cui, X.-S. Wei, and Z.-M. Chen, "Bbn: Bilateral-branch network with cumulative learning for long-tailed visual recognition," *arXiv preprint arXiv:1912.02413*, 2019.
- [56] A. van den Oord, Y. Li, and O. Vinyals, "Representation learning with contrastive predictive coding," *CoRR*, vol. abs/1807.03748, 2018.
- [57] Z. Wu, Y. Xiong, S. X. Yu, and D. Lin, "Unsupervised feature learning via non-parametric instance discrimination," in *CVPR*, 2018.
- [58] —, "Unsupervised feature learning via non-parametric instance discrimination," in *CVPR*, 2018.
- [59] R. Duggal, S. Freitas, S. Dhamnani, D. Horng, J. Sun *et al.*, "Elf: An early-exiting framework for long-tailed classification," *arXiv preprint arXiv:2006.11979*, 2020.
- [60] E. D. Cubuk, B. Zoph, J. Shlens, and Q. Le, "Randaugment: Practical automated data augmentation with a reduced search space," in *NeurIPS*, H. Larochelle, M. Ranzato, R. Hadsell, M. Balcan, and H. Lin, Eds., 2020.
- [61] K. Cao, C. Wei, A. Gaidon, N. Arechiga, and T. Ma, "Learning imbalanced datasets with label-distribution-aware margin loss," in *NeurIPS*, 2019.
- [62] X.-S. Wei, P. Wang, L. Liu, C. Shen, and J. Wu, "Piecewise classifier mappings: Learning fine-grained learners for novel categories with few examples," *IEEE TIP*, 2019.
- [63] N. Ma, X. Zhang, H. Zheng, and J. Sun, "Shufflenet V2: practical guidelines for efficient CNN architecture design," in *ECCV*, V. Ferrari, M. Hebert, C. Sminchisescu, and Y. Weiss, Eds., 2018.
- [64] A. Dosovitskiy, L. Beyer, A. Kolesnikov, D. Weissenborn, X. Zhai, T. Unterthiner, M. Dehghani, M. Minderer, G. Heigold, S. Gelly *et al.*, "An image is worth 16x16 words: Transformers for image recognition at scale," *arXiv preprint arXiv:2010.11929*, 2020.
- [65] T. Devries and G. W. Taylor, "Improved regularization of convolutional neural networks with cutout," *CoRR*, vol. abs/1708.04552, 2017.
- [66] E. D. Cubuk, B. Zoph, D. Mané, V. Vasudevan, and Q. V. Le, "Autoaugment: Learning augmentation strategies from data," in *CVPR*, 2019.
- [67] D. Hendrycks and T. G. Dietterich, "Benchmarking neural network robustness to common corruptions and surface variations," *arXiv preprint arXiv:1807.01697*, 2018.
- [68] D. Hendrycks, S. Basart, N. Mu, S. Kadavath, F. Wang, E. Dorundo, R. Desai, T. Zhu, S. Parajuli, M. Guo *et al.*, "The many faces of robustness: A critical analysis of out-of-distribution generalization," in *ICCV*, 2021, pp. 8340–8349.
- [69] H. Wang, S. Ge, Z. Lipton, and E. P. Xing, "Learning robust global representations by penalizing local predictive power," *Advances in Neural Information Processing Systems*, vol. 32, 2019.
- [70] M. Contributors, "MMSegmentation: Openmmlab semantic segmentation toolbox and benchmark," <https://github.com/open-mmlab/mmdetection>, 2020.
- [71] Z. Liu, Y. Lin, Y. Cao, H. Hu, Y. Wei, Z. Zhang, S. Lin, and B. Guo, "Swin transformer: Hierarchical vision transformer using shifted windows," in *ICCV*, 2021, pp. 10 012–10 022.
- [72] T. Xiao, Y. Liu, B. Zhou, Y. Jiang, and J. Sun, "Unified perceptual parsing for scene understanding," in *ECCV*, 2018, pp. 418–434.
- [73] W. Ouyang, X. Wang, C. Zhang, and X. Yang, "Factors in finetuning deep model for object detection with long-tail distribution," in *CVPR*, 2016.
- [74] X. Wang and G.-J. Qi, "Contrastive learning with stronger augmentations," 2021. [Online]. Available: https://openreview.net/forum?id=KJSC_AsN14
- [75] J. Cui, S. Liu, Z. Tian, Z. Zhong, and J. Jia, "Reslt: Residual learning for long-tailed recognition," *IEEE Transactions on Pattern Analysis and Machine Intelligence*, pp. 1–1, 2022.



Jiequan Cui received the B.Eng. degree from the computer science department of ShanDong University (SDU) in 2018. He is currently a Ph.D. Candidate at the Chinese University of Hong Kong (CUHK), under the supervision of Prof. Jiaya Jia. He serves as a reviewer for TPAMI, IJCV, CVPR, ICCV, ECCV, ICLR, NeurIPS. His research interests include model generalization and robustness, imbalanced learning, adversarial robustness, neural architecture search, and image segmentation.



Zhisheng Zhong received the B.Eng. Degree in Communication Engineering from Beijing University of Posts and Telecommunications (BUPT) in 2016. He received the Master Degree in Computer Science from Peking University (PKU) in 2019. Now he is a Ph.D. student at the Department of Computer Science Engineering (CSE), the Chinese University of Hong Kong (CUHK). He serves as a reviewer for NeurIPS, CVPR, ICCV, ICLR and etc. His research interests lie in deep learning and computer vision.



Zhuotao Tian received the B.Eng. degree (Honors) in Computer Science from the School of Computer Science and Technology, Harbin Institute of Technology (HIT) in 2018. He is currently a 3rd year Ph.D. student at the Chinese University of Hong Kong (CUHK), under the supervision of Prof. Jiaya Jia. He serves as a reviewer for IJCV, CVPR, ICCV, ECCV, AAAI. His research interests include few-shot learning, semi-supervised learning, semantic segmentation and scene text detection.



Shu Liu now serves as Co-Founder and Technical Head in SmartMore. He received the BS degree from Huazhong University of Science and Technology and the PhD degree from the Chinese University of Hong Kong. He was the winner of 2017 COCO Instance Segmentation Competition and received the Outstanding Reviewer of ICCV in 2019. He continuously served as a reviewer for TPAMI, CVPR, ICCV, NeurIPS, ICLR and etc. His research interests lie in deep learning and computer vision.



Bei Yu (Member, IEEE) received the Ph.D. degree from The University of Texas at Austin in 2014. He is currently an Associate Professor in the Department of Computer Science and Engineering, The Chinese University of Hong Kong. He has served as TPC Chair of ACM/IEEE Workshop on Machine Learning for CAD, and in many journal editorial boards and conference committees. He is Editor of IEEE TCCPS Newsletter. He received nine Best Paper Awards from DATE 2022, ICCAD 2021 & 2013, ASP-DAC 2021 & 2012, ICTAI 2019, Integration, the VLSI Journal in 2018, ISPD 2017, SPIE Advanced Lithography Conference 2016, and six ICCAD/ISPD contest awards.



Jiaya Jia received the Ph.D. degree in Computer Science from Hong Kong University of Science and Technology in 2004 and is currently a full professor in Department of Computer Science and Engineering at the Chinese University of Hong Kong (CUHK). He assumes the position of Associate Editor-in-Chief of IEEE Transactions on Pattern Analysis and Machine Intelligence (TPAMI) and is in the editorial board of International Journal of Computer Vision (IJCV). He continuously served as area chairs for ICCV,

CVPR, AAAI, ECCV, and several other conferences for the organization. He was on program committees of major conferences in graphics and computational imaging, including ICCP, SIGGRAPH, and SIGGRAPH Asia. He is a Fellow of the IEEE. V

Generalized Parametric Contrastive Learning

Supplementary Material

6 PROOF TO REMARK 1

For an image X_i and its label y_i , the expectation number of positive pairs with respect to X_i will be:

$$K_{y_i} = q(y_i) * (\text{length}(\text{queue}) + \text{batchsize} * 2 - 1) \approx \text{length}(\text{queue}) \cdot q(y_i), \quad (9)$$

$q(y_i)$ is the class frequency over the whole dataset. Here the " \approx " establishes because $\text{batchsize} \ll \text{length}(\text{queue})$ in training process. Note that we use such approximation just for simplification. Our analysis holds for the precise K_{y_i} . In what follows, we prove the optimal values for supervised contrastive loss.

Suppose training samples are i.i.d. To minimize the supervised contrastive loss for sample X_i , according to Eq. (3), we rewrite:

$$\begin{cases} P(i) = \{z_1^+, z_2^+, \dots, z_{K_{y_i}}^+\}; \\ p_i^+ = \frac{\exp(z_i^+ \cdot T(x_i))}{\sum_{z_k \in A(i)} \exp(z_k \cdot T(x_i))}; \\ p_{sum}^+ = p_1^+ + p_2^+ + \dots + p_{K_{y_i}}^+. \end{cases}$$

Then the supervised contrastive loss will be:

$$\begin{aligned} \mathcal{L}_i &= - \sum_{z_+ \in P(i)} \log \frac{\exp(z_+ \cdot T(x_i))}{\sum_{z_k \in A(i)} \exp(z_k \cdot T(x_i))} \\ &= -(\log p_1^+ + \log p_2^+ + \dots + \log p_{K_{y_i}}^+). \end{aligned}$$

For obtaining its optimal solution, we define the Lagrange multiplier form of \mathcal{L}_i as:

$$l = -(\log p_1^+ + \log p_2^+ + \dots + \log p_{K_{y_i}}^+) + \lambda(p_1^+ + p_2^+ + \dots + p_{K_{y_i}}^+ - p_{sum}^+), \quad (10)$$

where λ is the Lagrange multiplier. The first order conditions of Eq. (10) w.r.t. λ and p_i^+ can be written as follows:

$$\begin{cases} \frac{\partial l}{\partial p_i^+} = -\frac{1}{p_i^+} + \lambda = 0; \\ \frac{\partial l}{\partial \lambda} = p_1^+ + p_2^+ + \dots + p_{K_{y_i}}^+ - p_{sum}^+ = 0. \end{cases} \quad (11)$$

From Eq. (11), the optimal solution for p_i^* will be $\frac{p_{sum}^+}{K_{y_i}}$. Note that $p_{sum}^+ \in [0, 1]$, with a specific p_{sum}^+ , the minimal loss value of \mathcal{L}_i is:

$$\mathcal{L}_i = -K_{y_i} \log \frac{p_{sum}^+}{K_{y_i}}. \quad (12)$$

Thus, when $p_{sum}^+ = 1.0$, \mathcal{L}_i achieves minimum with the optimal value $p_i^+ = \frac{1}{K_{y_i}}$ which is exactly the probability that two samples of the same class are a true positive pair.

7 PROOF TO REMARK 2

For the image X_i and its label y_i , Eq. (9) still establishes for our parametric contrastive loss. To minimize the parametric contrastive loss for sample X_i , according to Eq. (4), we similarly rewrite:

$$\begin{cases} P(i) = \{z_1^+, z_2^+, \dots, z_{K_{y_i}}^+\} \\ p_i^+ = \frac{\exp(z_i^+ \cdot T(x_i))}{\sum_{z_k \in A(i) \cup \mathbf{C}} \exp(z_k \cdot T(x_i))} \\ p_c^+ = \frac{\exp(c_y \cdot T(x_i))}{\sum_{z_k \in A(i) \cup \mathbf{C}} \exp(z_k \cdot T(x_i))} \\ p_{sum}^+ = p_1^+ + p_2^+ + \dots + p_{K_{y_i}}^+ + p_c^+. \end{cases}$$

Then the parametric contrastive loss will be:

$$\mathcal{L}_i = \sum_{z_+ \in P(i) \cup \{c_y\}} -w(z_+) \log \frac{\exp(z_+ \cdot T(x_i))}{\sum_{z_k \in A(i) \cup \mathbf{C}} \exp(z_k \cdot T(x_i))} \quad (13)$$

$$= -\left(\log p_c^+ + \alpha \cdot (\log p_1^+ + \log p_2^+ + \dots + \log p_{K_{y_i}}^+)\right). \quad (14)$$

For obtaining its optimal solution, we define the Lagrange multiplier form of \mathcal{L}_i as:

$$l = -\left(\log p_c^+ + \alpha \cdot (\log p_1^+ + \log p_2^+ + \dots + \log p_{K_{y_i}}^+)\right) + \lambda(p_1^+ + p_2^+ + \dots + p_{K_{y_i}}^+ + p_c^+ - p_{sum}^+), \quad (15)$$

where λ is the Lagrange multiplier. The first order conditions of Eq. (15) w.r.t. λ , p_c^+ and p_i^+ can be written as follows:

$$\begin{cases} \frac{\partial l}{\partial p_i^+} = -\frac{\alpha}{p_i^+} + \lambda = 0; \\ \frac{\partial l}{\partial p_c^+} = -\frac{1}{p_c^+} + \lambda = 0; \\ \frac{\partial l}{\partial \lambda} = p_1^+ + p_2^+ + \dots + p_{K_{y_i}}^+ + p_c^+ - p_{sum}^+ = 0. \end{cases} \quad (16)$$

From Eq. (16), the optimal solution for p_i^+ and p_c^+ will be $\frac{\alpha p_{sum}^+}{1 + \alpha K_{y_i}}$ and $\frac{p_{sum}^+}{1 + \alpha K_{y_i}}$ respectively. Note that $p_{sum}^+ \in [0, 1]$, with a specific p_{sum}^+ , the minimal loss value of \mathcal{L}_i is:

$$\mathcal{L}_i = -\log \frac{p_{sum}^+}{1 + \alpha K_{y_i}} - \alpha K_{y_i} \log \frac{\alpha p_{sum}^+}{1 + \alpha K_{y_i}}. \quad (17)$$

Thus, when $p_{sum}^+ = 1.0$, \mathcal{L}_i achieves minimum with the optimal value $p_i^+ = \frac{\alpha}{1 + \alpha K_{y_i}}$, which is the probability that two samples of the same class are a true positive pair, and the optimal value $p_c^+ = \frac{1}{1 + \alpha K_{y_i}}$ which is the probability that a sample is closest to its corresponding center c_{y_i} among \mathbf{C} .

8 GRADIENT DERIVATION

In Section 3.4, we analyze PaCo loss under balanced setting, taking full ImageNet as an example. With P_{sup} increases from 0 to 0.71, the intensity of supervised contrastive loss will enlarge. Here we show that more samples will be pulled together with their corresponding centers when P_{sup} increases from 0 to 0.71 from the perspective of gradient derivation.

$$\frac{\partial \mathcal{L}}{\partial c_k} = \begin{cases} (\alpha K^* + 1)p_{c_k}x_i, & y_i \neq k; \\ \{(\alpha K^* + 1)p_{c_k} - 1\}x_i, & y_i = k. \end{cases} \quad (18)$$

It is worthy to note that when $p_{c_k} \in (0, 0.71)$, we have

$$\begin{cases} \frac{\partial \mathcal{L}}{\partial c_k} > 0, & y_i \neq k; \\ \frac{\partial \mathcal{L}}{\partial c_k} < 0, & y_i = k. \end{cases} \quad (19)$$

Eqs. (18) and (19) mean that as P_{sup} increases in training process, the probability that a sample is closest to its corresponding center will increase and the probability that a sample is closest to other centers will decrease. Thus, more and more samples will be pulled together with their right centers.

9 IMPLEMENTATION DETAILS FOR TABLE 1

We train models with cross-entropy, parametric contrastive loss 400 epochs without RandAugment respectively. For supervised contrastive loss, following the original paper, we firstly train the model 400 epochs. Then we fix the backbone and train a linear classifier 400 epochs.

10 MORE EXPERIMENTAL RESULTS ON MANY-SHOT, MEDIUM-SHOT, AND FEW-SHOT.

TABLE 16

Comprehensive results on ImageNet-LT with different backbone networks (ResNet-50, ResNeXt-50 & ResNeXt-101). Models are trained with RandAugment in 400 epochs. Inference time is calculated with a batch of 64 images on Nvidia GeForce 2080Ti GPU, Pytorch1.5, Python3.6.

Backbone	Method	Inference time (ms)	Many	Medium	Few	All
ResNet-50	τ -normalize	8.3	65.0	52.2	32.3	54.5
	Balanced Softmax	8.3	66.7	52.9	33.0	55.0
	PaCo	8.3	65.0	55.7	38.2	57.0
	GPaCo	8.3	66.1	57.3	40.2	58.5
ResNeXt-50	τ -normalize	13.1	66.4	53.4	38.2	56.0
	Balanced Softmax	13.1	67.7	53.8	34.2	56.2
	PaCo	13.1	67.5	56.9	36.7	58.2
	GPaCo	13.1	67.4	57.1	41.2	58.9
ResNeXt-101	τ -normalize	25.0	69.0	55.1	36.9	57.9
	Balanced Softmax	25.0	69.2	55.8	36.3	58.0
	PaCo	25.0	68.2	58.7	41.0	60.0
	GPaCo	25.0	68.7	59.5	42.8	60.8

TABLE 17

Comprehensive results on ImageNet-LT with RIDE. Models are trained with RandAugment in 400 epochs. Inference time is calculated with a batch of 64 images on Nvidia GeForce 2080Ti GPU, Pytorch1.5, Python3.6.

Backbone	Method	Inference time (ms)	Many	Medium	Few	All
RIDEResNet	1 expert	8.2	64.8	49.8	29.6	52.8
	2 experts	12.0	67.7	53.5	31.5	56.0
	3 experts	15.3	69.0	54.7	32.5	57.0
RIDEResNeXt	1 expert	13.0	67.2	49.0	28.1	53.2
	2 experts	19.0	70.4	52.6	30.3	56.4
	3 experts	26.0	71.8	53.9	32.0	57.8

TABLE 18

Comprehensive results on iNaturalist 2018 with ResNet-50 and ResNet-152. †represents the models are trained without RandAugment. Inference time is calculated with a batch of 64 images on Nvidia GeForce 2080Ti GPU, Pytorch1.5, Python3.6.

Backbone	Method	Inference time (ms)	Many	Medium	Few	All
ResNet-50	τ -normalize	8.3	74.1	72.1	70.4	71.5
	Balanced Softmax	8.3	72.3	72.6	71.7	71.8
	PaCo	8.3	70.3	73.2	73.6	73.2
ResNet-50 †	Balanced Softmax	8.3	72.5	72.3	71.4	71.7
	PaCo	8.3	69.5	73.4	73.0	73.0
	GPaCo	8.3	73.1	75.4	75.9	75.4
ResNet-152	PaCo	20.1	75.0	75.5	74.7	75.2

TABLE 19

Comprehensive results on iNaturalist 2018 with RIDE. Models are trained with RandAugment in 400 epochs without knowledge distillation. Inference time is calculated with a batch of 64 images on Nvidia GeForce 2080Ti GPU, Pytorch1.5, Python3.6.

Backbone	Method	Inference time (ms)	Many	Medium	Few	All
RIDEResNet	1 expert	8.2	56.0	66.3	66.0	65.2
	2 experts	12.0	62.2	70.5	70.0	69.5
	3 experts	15.3	66.5	72.1	71.5	71.3